J. Fluid Mech. (1975), *vol.* 67, *part* 2, *pp.* 257–271
Printed in Great Britain

Scaling laws for pipe-flow turbulence

By A. E. PERRY AND C. J. ABELL†
Department of Mechanical Engineering, University of Melbourne, Parkville, Australia

(Received 7 August 1973 and in revised form 23 May 1974)

Using hot-wire-anemometer dynamic-calibration methods, fully developed pipe-flow turbulence measurements have been taken in the Reynolds-number range 80×10^3 to 260×10^3. Comparisons are made with the results of previous workers, obtained using static-calibration methods. From the dynamic-calibration results, a consistent and systematic correlation for the distribution of turbulence quantities becomes evident, the resulting correlation scheme being similar to that which has previously been established for the mean flow. The correlations reported have been partly conjectured in the past by many workers but convincing experimental evidence has always been masked by the scatter in the results, no doubt caused by the difficulties associated with static-calibration methods, particularly the earlier ones. As for the mean flow, the turbulence intensity measurements appear to collapse to an inner and outer law with a region of overlap, from which deductions can be made using dimensional arguments. The long-suspected similarity of the turbulence structure and its consistency with the established mean-flow similarity appears to be confirmed by the measurements reported here.

1. Introduction

The axisymmetric fully developed flow of air in a pipe provides one of the simplest and most reproducible laboratory flows for experimental wall-turbulence studies. However, all turbulence-structure hypotheses developed to date have relied upon experimental results which show considerable inconsistencies. For example, the studies of Laufer (1954), Morrison & Kronauer (1968), Townes *et al.* (1971) and Lawn (1971) show differences in the reported r.m.s. turbulence level of up to 25%.

The authors feel that the inconsistencies shown in previous data are due to several factors, including an insufficient flow development length, ill-conditioned hot-wire-anemometer calibration methods, inaccuracy in wall-distance measurements, failure to observe the wire filament and its position while measurements are being taken, and difficulties associated with the accurate alignment of hot-wire probes. The present work was undertaken with the aim of minimizing errors due to the above factors to obtain consistent pipe-flow turbulence data.

† Present address: Engineering Department, University of Cambridge.

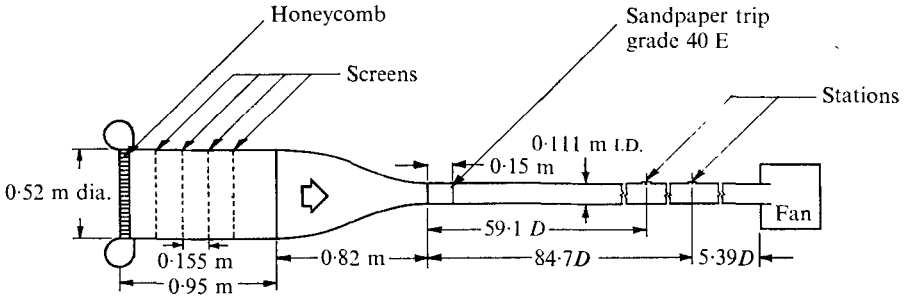

FIGURE 1. Apparatus. D is internal diameter.

2. Experimental methods and apparatus

All results were obtained in the apparatus shown diagramatically in figure 1. The pipe used was precision-drawn brass tubing of diameter 11·1 cm and 10 m long. The inlet contraction was fitted with an hexagonal honeycomb of cell width-to-length ratio 7 and cell size 9·5 mm. The four screens shown are of gauges 24, 25, 26 and 28 respectively in the streamwise direction. A sandpaper trip was used after the contraction to stabilize the flow transition.

The measurements reported here were taken at stations 71·9 and 84·7 diameters from the pipe entrance.

2.1. *Mean-flow characteristics*

All mean-flow profiles were measured using traversing total-head tubes and wall static-pressure tappings. This method is more direct and accurate than hot-wire techniques when using unlinearized anemometers and avoids the need for repeated calibrations. The mean profiles are shown in figure 2 in the form of a velocity defect $(U_1 - U)/u_\tau$, where U_1 is the centre-line velocity, U the local mean velocity and u_τ the shear velocity. The velocity defect shows good collapse with no systematic Reynolds-number variation away from the wall.

The shear velocity u_τ was estimated from a Clauser chart (Clauser 1954) using the logarithmic law proposed by Coles (1968):

$$U/u_\tau = (0{\cdot}41)^{-1} \ln y^+ + 5{\cdot}0, \tag{1}$$

where $y^+ = yu_\tau/\nu$, y is the wall distance and ν the kinematic viscosity. Combining (1) with the velocity defect law leads to the more general form

$$U/u_\tau = (0{\cdot}41)^{-1} \ln y^+ + 5{\cdot}0 + h[y/R] \tag{2}$$

for $y^+ > 100$ and $y/R \leqslant 1$ (where R is the pipe radius).

Ferriss (1965) has shown that slight tapers in the duct cross-section have a marked influence on pressure-drop measurements, and hence on the inferred values of u_τ. Nevertheless, values of u_τ deduced from pressure-drop measurements agreed with Clauser-chart values to within 3%.

Figure 3 shows typical mean-flow results compared with (1). Values of u_τ/U_1 were interpolated where necessary from the skin-friction law given by (2) with $y = R$ and with the measured value of the centre-line 'deviation' h[1].

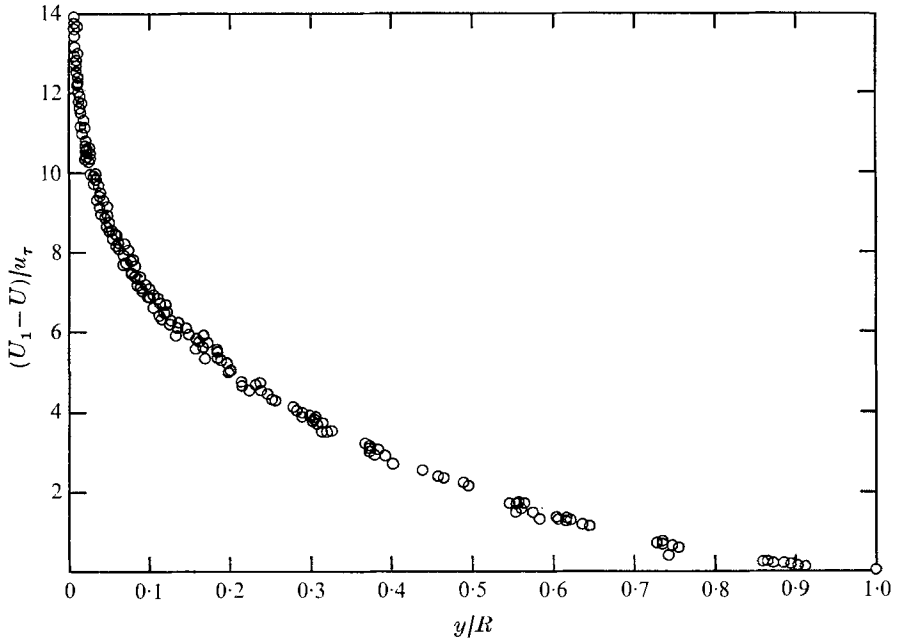

FIGURE 2. Velocity defect of mean-flow results. Reynolds-number range is 80×10^3 to 350×10^3.

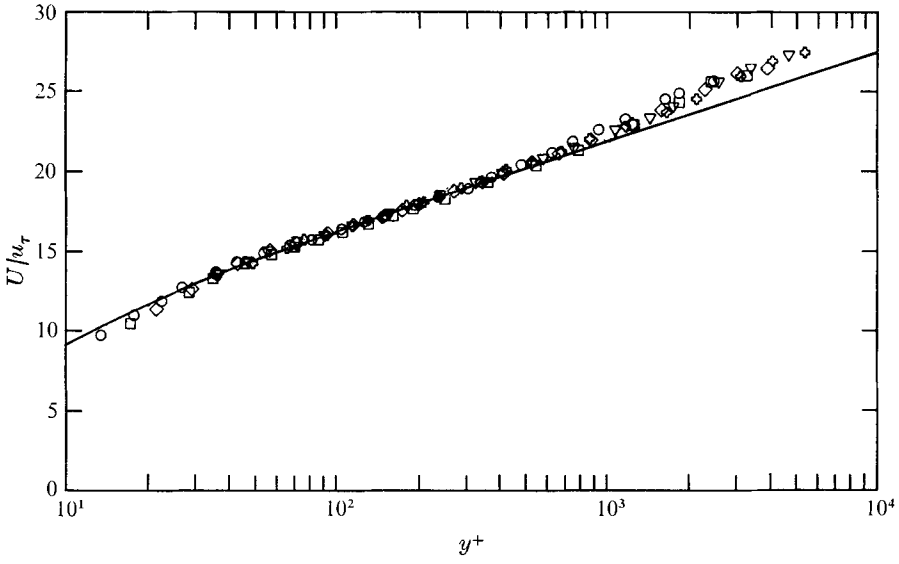

FIGURE 3. Typical mean-flow profiles compared with logarithmic law of the wall, with buffer region according to Squire (1948).

	○	□	◇	▽	✣
$Re \times 10^{-3}$	128·4	170·5	212·5	255·5	296·5

The existence of fully developed flow was ensured by comparing local mean velocity profiles and r.m.s. longitudinal turbulence measurements $\tilde{u}'$ at the two measuring stations. The flow was also checked for a possible lack of axisymmetry caused by entry conditions by measuring $\tilde{u}'$ at fixed radii and rotating the entrance assembly relative to the pipe. The flow was found to be axisymmetric and fully developed at and beyond 71·9 diameters downstream up to a Reynolds number of 350×10^3 based on the pipe diameter and centre-line velocity.

2.2. *Turbulence measurements*

Unlinearized constant-temperature anemometer equipment was used throughout, the design being similar to that described in Perry & Morrison (1971*a*). For longitudinal turbulence measurements, DISA 55 F14 probes were used with the authors' filaments, consisting of 4 μm diameter platinum wires (Wollaston type). Typical etched lengths were 1·2–1·5 mm. Measurements of Reynolds stress and transverse turbulence were taken using DISA 55 A38 cross-wire probes with the manufacturers' 5 μm diameter tungsten wires, 1·2 mm long.

Dynamic-calibration methods were used for all turbulence intensity and correlation measurements.

For normal wires, the small-perturbation sensitivity $s = \tilde{e}'/\tilde{u}'$ (where $\tilde{e}'$ is the r.m.s. voltage perturbation anemometer output) was measured directly by oscillating the probe sinusoidally in a steady flow. This enabled the velocity sensitivity of the entire hot-wire system from probe filament to DVM output to be obtained without recourse to any heat-transfer law, curve fitting or numerical differentiation methods.

Cross-wire probes were calibrated by subjecting the probe to both longitudinal and transverse velocity perturbations in turn. Using this technique, no assumptions regarding wire angles or matching of the two wires of the probe and their respective anemometer channels were required. All calibration and signal processing was accomplished using EAI TR20 and TR48 analog computers, all fitted with TR 48 amplifiers. The dynamic-calibration methods are described in detail by Perry & Morrison (1971*b*) and Morrison, Perry & Samuel (1972).

The possibility of hot-wire calibration drift due to wire ageing and contamination meant that all wires had to be calibrated both before and after use to check for constant characteristics. If the two calibrations of a given wire failed to agree in sensitivity to within better than 2 % then the data obtained using that wire were rejected.

The anemometer frequency response was checked and adjusted using square-wave injection to ensure a quadratic pole of optimum damping at or beyond 20 kHz for all measurements.

Since the operating point of the anemometer was defined by the mean output voltage $\bar{E}$ the results were corrected where necessary for changes in the ambient temperature θ between calibration and measurement using the partial derivative $[s^{-1}\,\partial s/\partial\theta]_{\bar{E}}$, calculated from the heat-transfer law of Grant & Kronauer (1962). Typical temperature corrections were of the order of 2 %.

Energy spectra of the longitudinal component of turbulence were measured

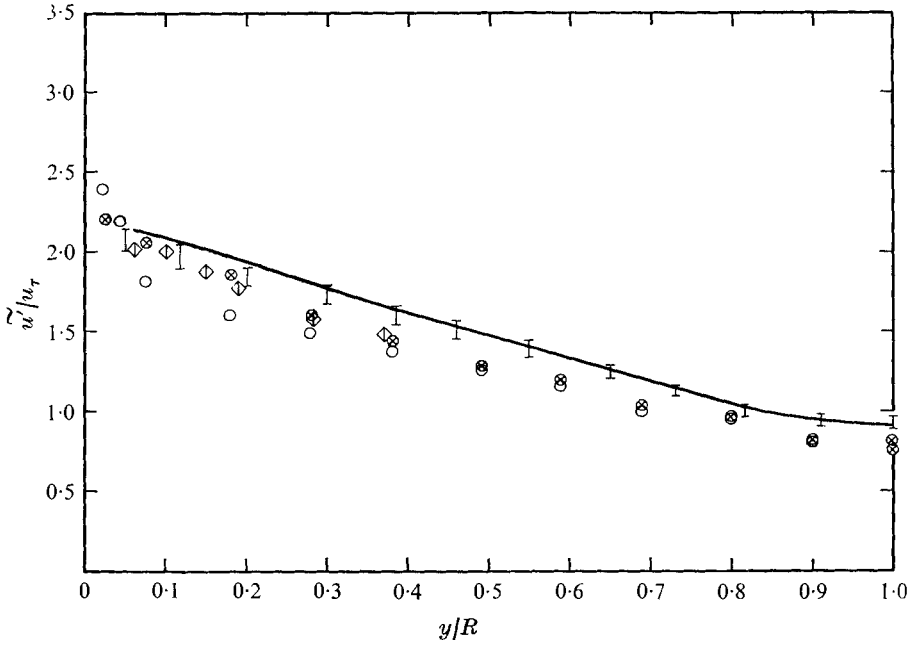

FIGURE 4. Comparison of 'outer flow' longitudinal turbulence data with results of some earlier workers. ——, mean curve fitted to data of figure 6, $78 \times 10^3 \leqslant Re \leqslant 257 \times 10^3$; I, Lawn, $38 \times 10^3 \leqslant Re \leqslant 250 \times 10^3$; ◇, Morrison & Kronauer, $34 \times 10^3 \leqslant Re \leqslant 193 \times 10^3$; ⊗, Laufer, $Re = 500 \times 10^3$; ○, Laufer, $Re = 50 \times 10^3$.

using two Krohn-Hite filters (model 3321), compounded to give a bandpass of approximately one third of an octave. For spectral measurements, wires of active length 1·2–1·3 mm were used.

2.3. *Wall-distance measurement*

To obtain wall-distance estimates of sufficient accuracy, a short-focusing telescope was used to give successive readings of the separation of the wire and its image in the polished wall for various transverse positions (measured on a micrometer head). Since the active sections of hot wires bow owing to thermal expansion, a telescope of sufficient magnification to view the etched section of the wire and its image had to be used. Using this method, 95% confidence limits gave an uncertainty in wall distance of typically $\pm 0{\cdot}04$ mm.

3. Experimental measurements

3.1. *Longitudinal turbulence*

The root-mean-square longitudinal turbulence $\tilde{u}'$ was measured at four Reynolds numbers ranging from 78×10^3 to 257×10^3. Owing to wall proximity effects (see Wills 1962), measurements were not taken closer than 0·4 mm or 80 wire diameters from the wall. This represents y^+ values of 12 for the lowest Reynolds number and 35 for the highest. The data are presented in figures 4–7. Figures 4 and 5 compare the data reported here with those of some previous workers.

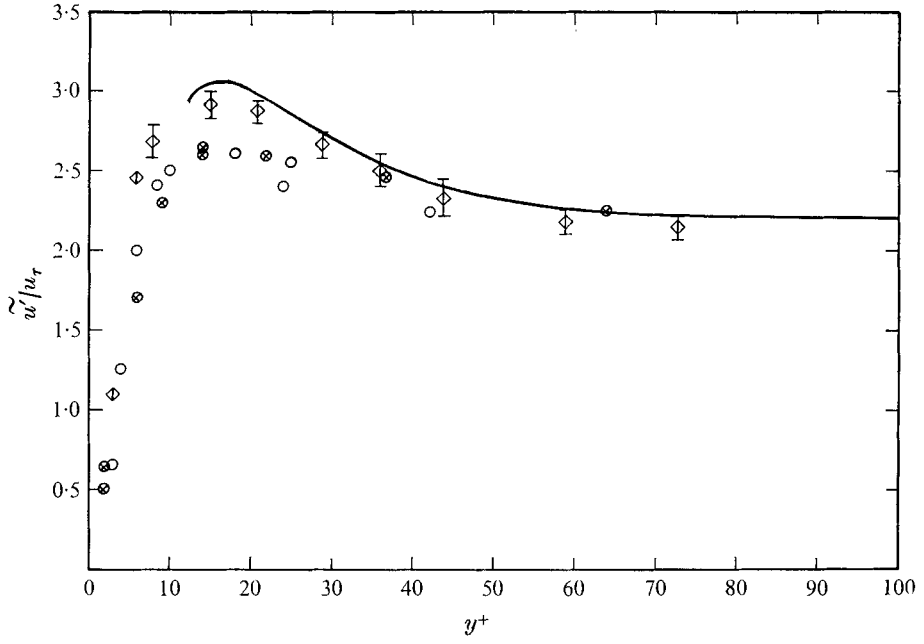

FIGURE 5. Comparison of 'inner flow' longitudinal turbulence data with results of some earlier workers. ——, mean curve fitted to data of figure 7; ⧱, Morrison & Kronauer, $34 \times 10^3 \leqslant Re \leqslant 193 \times 10^3$; ⊗, Laufer, $Re = 500 \times 10^3$; ○, Laufer, $Re = 50 \times 10^3$.

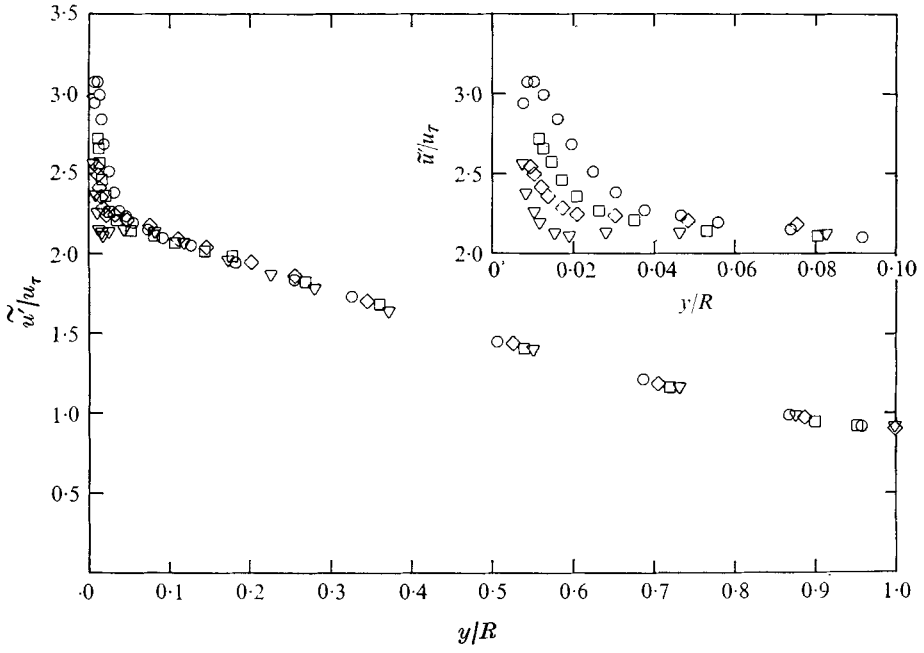

FIGURE 6. Longitudinal turbulence results for outer flow.

	Re	u_τ/U_1
○	78×10^3	0·0411
□	133×10^3	0·0392
◇	173×10^3	0·0383
▽	257×10^3	0·0370

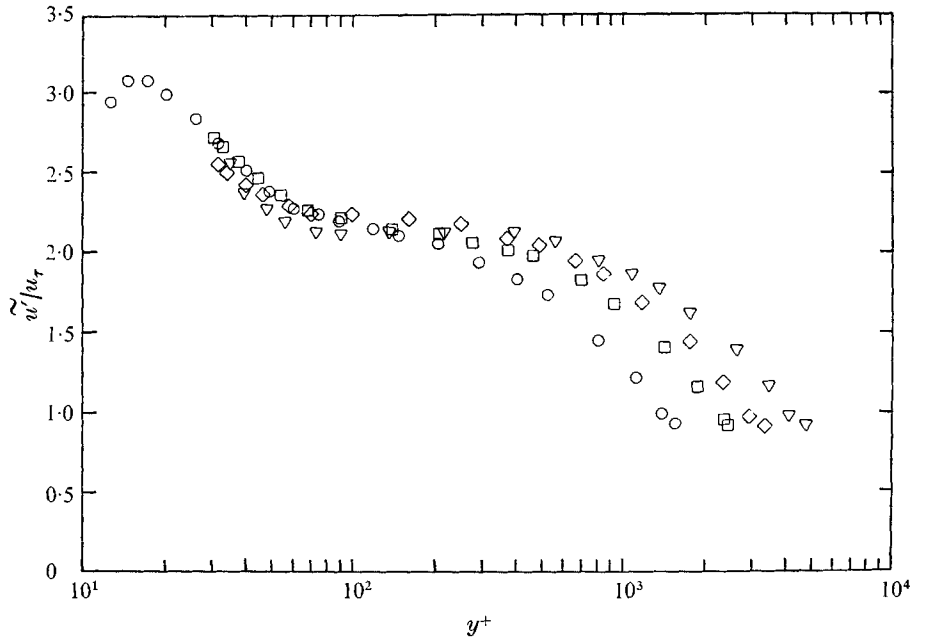

FIGURE 7. Longitudinal turbulence data. Symbols as for figure 6.

The 'outer flow' data presented in figure 6 show a good collapse of the turbulence level $\tilde{u}'/u_\tau$ for all the Reynolds numbers examined for $y/R > 0{\cdot}1$, as suggested by Townsend's (1956, p. 89) hypothesis of Reynolds-number similarity of the outer flow. The inset in figure 6 shows that for $y/R < 0{\cdot}1$ the data have no tendency to collapse as a function of non-dimensional wall distance y/R. However, as seen from figure 7, the same data close to the wall correlate well as $\tilde{u}'/u_\tau$ *vs.* y^+ for $y/R < 0{\cdot}1$, indicating the existence of an inner-region scaling with inner-flow variables. An important consequence of plotting the data this way is that distinct regions of constant turbulence level $\tilde{u}'/u_\tau$ appear. Regions of constant $\tilde{u}'/u_\tau$ are consistent with an overlap of inner and outer laws. If a function $f_0[y/R]$† describing the outer flow is to extend over a region where the turbulence is also described by $\tilde{u}'/u_\tau = f_i[y^+]$, then $\tilde{u}'/u_\tau$ must be a universal constant, since the arguments y^+ and y/R are arbitrarily independent variables. Further, it is enlightening to show the mean-flow profiles on the same graph as the turbulence data, as in figure 8, where all data are shown as faired curves. The spatial extent λ of constant turbulence level and logarithmic mean flow are seen to correspond well.

The data presented in figures 6 and 7 have not been corrected for the effect of finite wire length, but corrections to the r.m.s. longitudinal turbulence broad-band measurements based on measured spectra using the method of Wyngaard (1968) are less than 3% at $y^+ = 100$, decreasing to 1% for $y/R > 0{\cdot}2$.

† Throughout this paper, square brackets indicate a functional dependence.

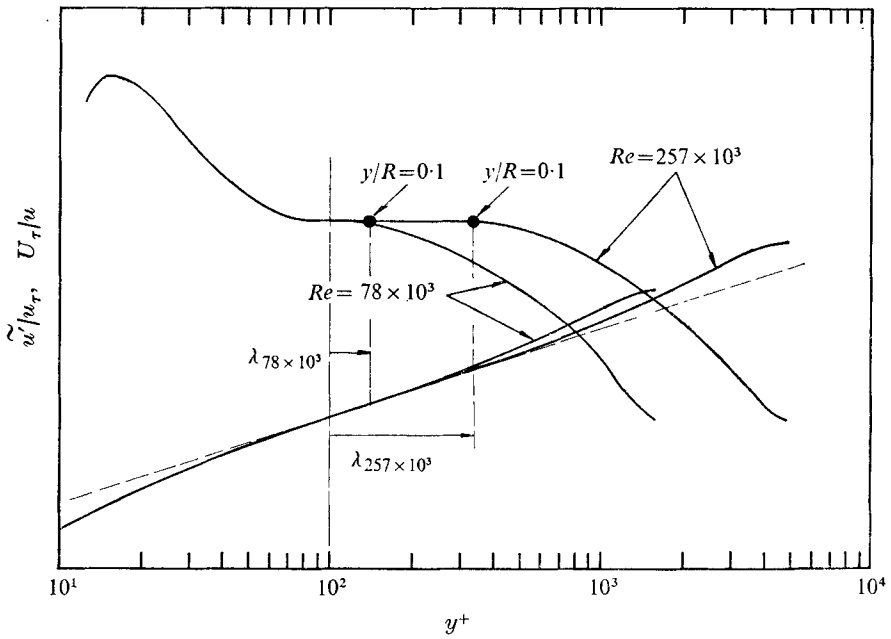

FIGURE 8. Spatial comparison between regions of constant longitudinal turbulence level and logarithmic mean flow for $Re = 78 \times 10^3$ and 257×10^3.

3.2. *Transverse turbulence and Reynolds stress*

Measurements of the r.m.s. transverse turbulence $\tilde{v'}$ and kinematic Reynolds stress $-\overline{u'v'}$ were taken at Reynolds numbers of 100×10^3 and 200×10^3, using cross-wire probes. Results obtained using cross-wire probes are subject to several sources of error. First, approximately 2·5 % and 5 % errors in deduced values of $\overline{v'^2}$ and $\overline{u'v'}$ respectively result from a rotation of the probe of 1° about the normal to the plane of the crossed wires, relative to a mean streamline (pitch-angle variation). Second, movement of the hot-wire filament causes a considerable change in the effective angle of the wire to the mean flow, and hence a large change in velocity sensitivity. When a wire is bowed by thermal expansion, lateral aerodynamic forces can cause the bowing to move (Perry & Morrison 1971*c*). If there is any plastic bending in the filament, this deflexion will have a hysteresis. That is, as the wire is unloaded, its movement may not be reversible. The authors have on many occasions observed two distinct calibration curves for the same inclined wire, each corresponding to a different position of the wire filament. Hence it would appear that for cross-wire measurements in situations where it is not possible to check the probe pitch angle directly, or monitor the wire filament position, dynamic-calibration methods are as unreliable as static-calibration methods. A further source of error for inclined wires arises from slight inaccuracies in the analog computer scaling used to convert the voltage signals to velocity correlations. This source is always present irrespective of the calibration method and reflects the ill-conditioned nature of the inclined-wire equations being used in the signal processing.

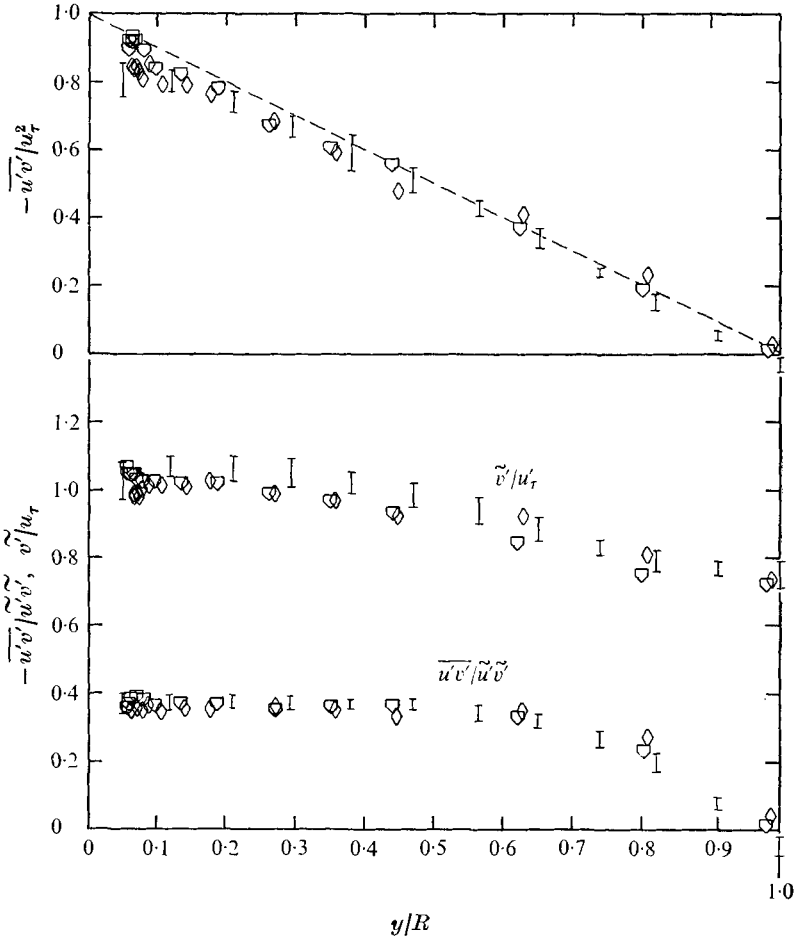

FIGURE 9. Cross-wire measurements. ▽, $Re = 100 \times 10^3$, $u_\tau/U_1 = 0{\cdot}0402$; ◇, $Re = 200 \times 10^3$, $u_\tau/U_1 = 0{\cdot}0387$; I, Lawn, $38 \times 10^3 \leqslant Re \leqslant 250 \times 10^3$.

Figure 9 shows the data obtained for the correlation $-\overline{u'v'}/u_\tau^2$, transverse turbulence $\tilde{v}'/u_\tau$ and correlation coefficient $-\overline{u'v'}/\tilde{u}'\tilde{v}'$, together with the data of Lawn. The data have not been corrected for finite wire length.

The error in the $\tilde{u}'/u_\tau$ results obtained using cross-wire probes compared with those obtained using normal wires (§3.1) is of the same order ($\pm 5\%$) as the difference between the $\tilde{v}'/u_\tau$ results at the two Reynolds numbers. Taking this into account, Reynolds-number similarity of the outer flow for transverse turbulence would seem plausible. This is also supported by the small variation of the correlation coefficient and the data of Lawn.

3.3. *Energy spectra of longitudinal turbulence*

The following definitions for the spectrum functions will be used:

$$\Phi[\omega', x_1, x_2, \ldots] \quad \text{and} \quad \phi[\omega', x_1, x_2, \ldots]$$

are chosen so that $$\int_0^\infty \Phi[\omega', x_1, x_2, \ldots]\, d\omega' = \left(\frac{\tilde{u}'}{u_\tau}\right)^2 [x_1, x_2, \ldots] \tag{3}$$

and $$\int_0^\infty \phi[\omega', x_1, x_2, \ldots]\, d\omega' = 1. \tag{4}$$

Also $$\Psi[\omega', x_1, x_2, \ldots] = \omega' \Phi[\omega, x_1, x_2, \ldots] \tag{5}$$

and $$\psi[\omega', x_1, x_2, \ldots] = \omega' \phi[\omega', x_1, x_2, \ldots]. \tag{6}$$

The functions Ψ and ψ are more convenient in form from an experimental viewpoint since constant-percentage bandwidth filters have been used. The variable ω' is a non-dimensional circular frequency to be chosen differently in the inner and outer regions (see below), and x_1, x_2, etc., are further non-dimensional parameters.

In the viscosity-dependent region close to the boundary, it is proposed that

$$\Phi = \Phi[\omega\nu/u_\tau^2, yu_\tau/\nu]. \tag{7}$$

This is consistent with the 'law of the wall' philosophy in that, as for the mean flow and the broad-band turbulence distributions close to the boundary, outer-flow variables R and U_1 are not the pertinent scales. Note that here $\omega' = \omega\nu/u_\tau^2$.

For the outer flow, if the observer were moving with a velocity U_1, then to be consistent with the hypothesis of Reynolds-number similarity,

$$\Phi = \Phi[\omega y/u_\tau, y/R]. \tag{8}$$

That is, neither the viscosity nor the velocity of the observer relative to the boundary enters the problem explicitly. However, since the observer is stationary, an additional parameter is necessary to account for the convection of the turbulence structure past the observer. Hence, for the outer flow, three parameters are required, and it will be seen later that it is convenient to use the following:

$$\Phi = \Phi[\omega y/U, y/R, U_1/u_\tau], \tag{9}$$

i.e. $\omega' = \omega y/U$ for the outer spectra. Of course, at very high wavenumbers, these similarity arguments must break down, since viscous effects become important. However, this does not detract from the validity of (7) and (9) concerning the energy-containing motions.

Longitudinal turbulence spectra were measured for varying wall distance at Reynolds numbers of 80×10^3, 120×10^3, 180×10^3 and 260×10^3. Representative spectra are shown in figure 10(*a*) as ψ *vs.* $\omega y/U$ for varying wall distance y/R. It is seen that the data plotted in this form are independent of Reynolds number for $y^+ > 100$. Closer to the wall (corresponding to $y^+ < 100$) the spectral shapes are dissimilar for different Reynolds numbers, when plotted as ψ *vs.* $\omega y/U$, as seen in figure 10(*b*).

Further, a region where the spectrum function ψ *vs.* $\omega y/U$ does not change with wall distance appears for $y/R < 0{\cdot}1$ and $y^+ > 100$. This corresponds to the region of overlap. Spectral measurements taken within the overlap region $y^+ > 100, y/R < 0{\cdot}1$ are shown in figure 11(*a*) plotted as Ψ *vs.* $\omega y/U$. All the data obtained within this region comprise 10 spectra at 9 values of y^+ at four Reynolds numbers. Figure 11(*b*) shows the same data plotted as Ψ *vs.* $\omega\nu/u_\tau^2$. Although marginal, a comparison of the two figures indicates that the more pertinent non-dimensional parameter is probably $\omega y/U$. That is, within this region,

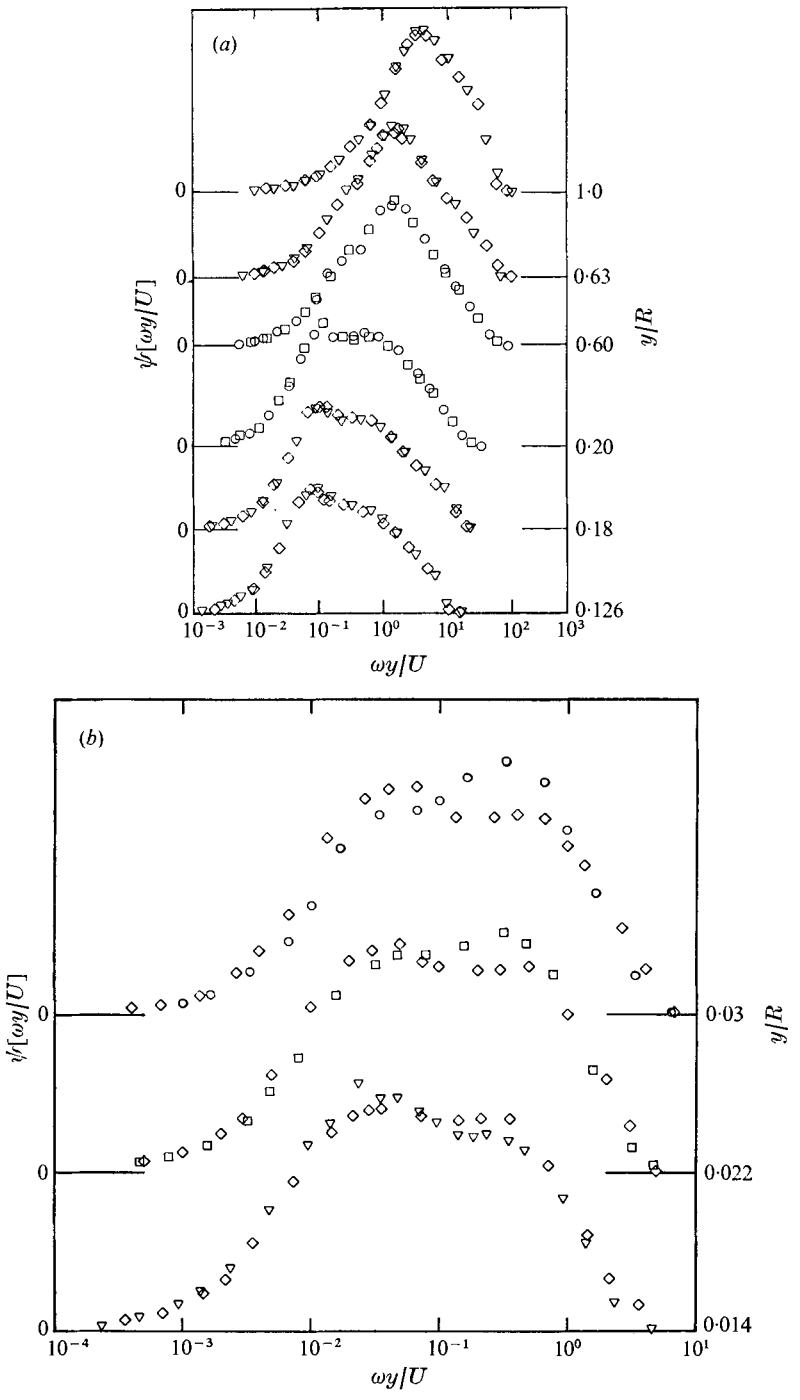

FIGURE 10. Longitudinal turbulence spectra for varying wall distance. (*a*) $y^+ > 100$. (*b*) $y^+ < 100$.

	Re	u_τ/U_1
○	80×10^3	0·0410
□	120×10^3	0·0396
◇	180×10^3	0·0381
▽	260×10^3	0·0370

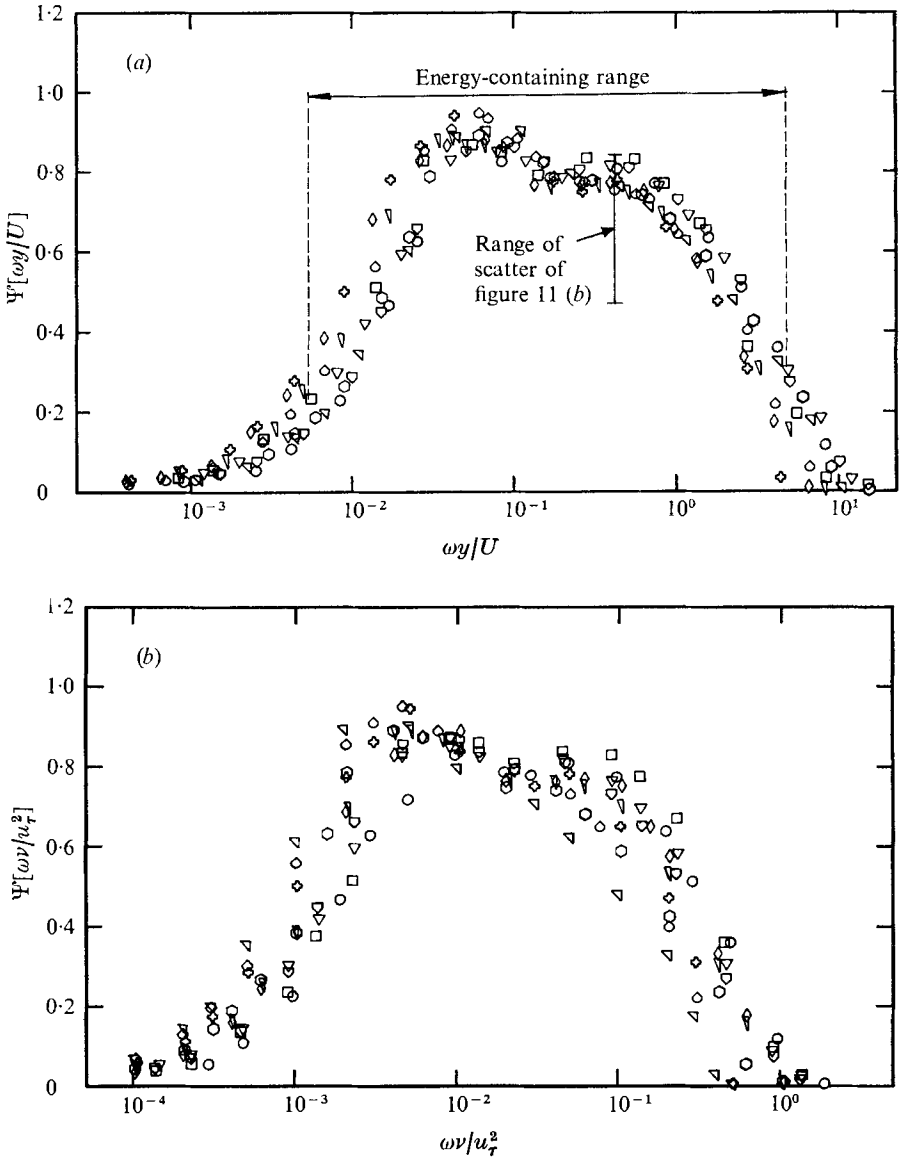

FIGURE 11. Longitudinal turbulence spectrum within region of constant $\tilde{u}'/u_\tau$.

	$Re \times 10^{-3}$	y^+	y/R	U/u_τ
○	80	150	0·0934	17·6
□	120	100	0·043	16.6
▽	120	150	0·0645	17.59
▽	120	200	0·086	18·3
◇	180	104	0·03	16·6
◁	180	138	0·04	17·31
◇	180	275	0·08	19·2
✣	260	148	0·03	17·6
⬠	260	246	0·05	18·8
◁	260	444	0·09	20·4

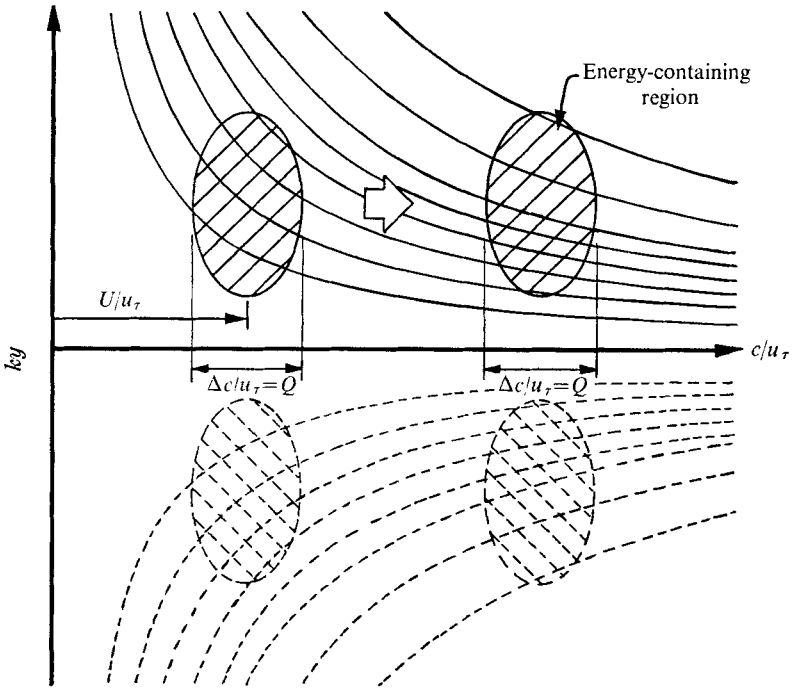

FIGURE 12. Spectrum function $W(ky, c/u_\tau)$. The arrow shows the translation of $W(ky, c/u_\tau)$ contour for increasing Reynolds number and/or increasing y^+ within the region of overlap. Q is a universal constant representing the non-dimensional spread of the phase velocity associated with the contour shown.

$\Psi = \Psi[\omega y/U]$, approximately a universal spectrum function. It is conjectured by the authors in what follows that a more precise universality of the spectrum function would occur in the region of overlap if wavenumber/phase-velocity concepts were used.

The scaling of frequency with wall distance and local mean velocity to give a universal function within this region of overlap can be deduced from dimensional arguments. Within the region of constant $\tilde{u}'/u_\tau$, it can be seen from the previous results that the length scales ν/u_τ and R do not control the characteristic scale of the energy-containing components. The only length scale remaining is the wall distance y. Also, the representation of the spectrum of the energy-containing turbulence in the wavenumber (k), phase velocity (c) plane within this region has a spread of phase velocities scaling with u_τ (see figure 12). This is consistent with the Townsend hypothesis of Reynolds-number similarity for the outer flow: all mean relative motions and energy-containing turbulence motions have one characteristic velocity scale, namely u_τ. It can be shown from the relationship between the space–time correlation and its Fourier transform expressed in terms of phase velocity and wavenumber

$$W[k, c] = (2\pi)^{-2} \int\int_{-\infty}^{\infty} R[\delta, \tau] \exp\{ik(\delta - c\tau)\} d\delta\, d\tau \tag{10}$$

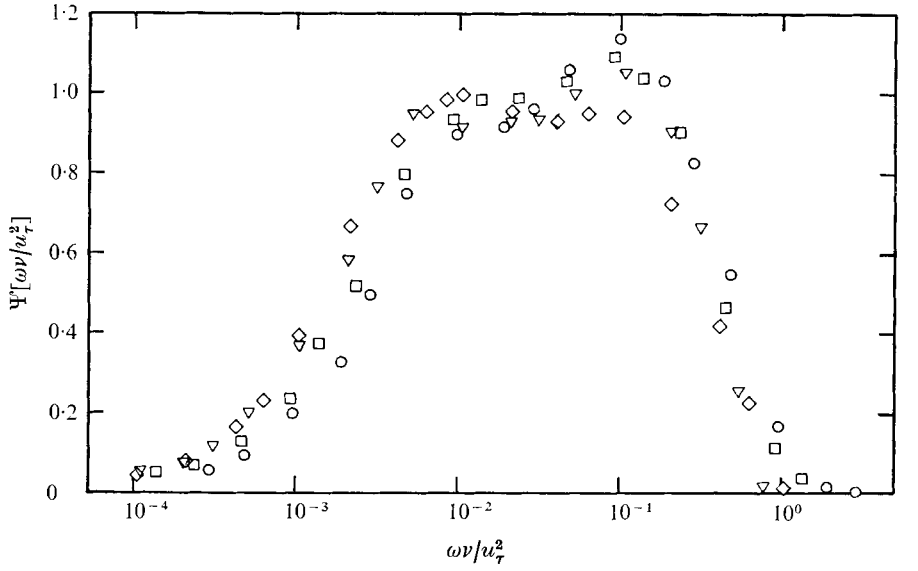

FIGURE 13. Longitudinal turbulence spectra. $y^+ = 50$.

	Re	u_τ/U_1		Re	u_τ/U_1
○	80×10^3	0·0410	◇	180×10^3	0·0381
□	120×10^3	0·0396	▽	260×10^3	0·0370

(see Wills 1964) that, if W_V is the spectrum seen by an observer moving with velocity V, and W_0 the spectrum seen by a stationary observer,

$$W_V[k, c] = W_0[k, c - V]. \tag{11}$$

This means that the contours of $W[k, c]$ shown in figure 12 translate without distortion for change of the velocity of the observer relative to the turbulent field. Higher-Reynolds-number flow hence leads to a reduced fractional spread $\Delta c/U$ of phase velocities as seen by a stationary observer, and Taylor's hypothesis of a frozen convected turbulence structure becomes more accurate, since within the region where most of the energy is located (shown shaded in figure 12), the hyperbolic contours corresponding to constant frequency ω become more closely contours of constant wavenumber k, with $\omega = kU$. At lower Reynolds numbers this approximation breaks down and this could partially explain the scatter in figure 11 (*a*).

The spectral correlation shown in figure 11 (*a*) has been suggested previously by other workers, for example, Morrison & Kronauer (1968).

Figure 13 shows typical data obtained for $y^+ < 100$ plotted as Ψ *vs.* $\omega\nu/u_\tau^2$ for a y^+ value of 50. The small variation between results at different Reynolds numbers is encouraging since the spectral shape is strongly dependent on wall distance close to the wall. The results suggest that $\Psi = \Psi\,[\omega\nu/u_\tau^2, yu_\tau/\nu]$ as anticipated earlier from the 'law of the wall' philosophy.

For the detailed results obtained in the outer flow, refer to figure 10 (*a*). The spectra show good agreement between results for different Reynolds numbers at the same y/R, indicating that the Reynolds number has a relatively minor

effect on the spectrum function. The reason for this could be that the fractional spread of phase velocities is small. In any case, U_1/u_τ is a weak function of Reynolds number.

4. Discussion and conclusions

It has been shown here that by using the hot-wire-anemometer dynamic-calibration techniques of Perry & Morrison (1971*a*), a consistent correlation for pipe-flow turbulence structure becomes apparent. The longitudinal turbulence, like the mean-flow velocity, follows an inner flow/outer flow law with a corresponding region of overlap. From the form of the inner and outer regions, the overlap can be predicted as a region of constant and universal value of $\tilde{u'}/u_\tau$. This agrees with measurements in the wall-distance range $y^+ > 100$, $y/R < 0{\cdot}1$.

Transverse turbulence results indicate that an outer-flow behaviour similar to that observed for the longitudinal turbulence is plausible.

Also, from the inner and outer flow structure of the turbulence, certain properties relating to the spectra can be deduced. The most important of these is that, in the region of constant $\tilde{u'}/u_\tau$ at the Reynolds numbers measured, the characteristic wavenumber scales with the wall distance and Taylor's hypothesis becomes more accurate with increased Reynolds number.

The location by broad-band measurements of the critical regions for which spectra should be measured has helped to rationalize spectral correlations. In the past, too few spectra have been taken in the zone $y^+ > 100$, $y/R < 0{\cdot}1$ and spectra measured outside this region were being compared to those measured within the region, leading to considerable confusion as to which parameters were controlling the flow.

REFERENCES

Clauser, F. H. 1954 *J. Aero. Sci.* **21**, 91.

Coles, D. E. 1968 *Proc. AFOSR-IFP-Stanford Conf. on Computation of Turbulent Boundary Layers* (ed. D. E. Coles & E. A. Hirst), vol. 2, p. 1.

Ferriss, D. H. 1965 *Aero. Res. Counc. Current Paper*, no. 831.

Grant, H. P. & Kronauer, R. E. 1962 *Symp. on Measurement in Unsteady Flow, A.S.M.E.*

Laufer, J. 1954 *N.A.C.A. Tech. Rep.* no. 1174.

Lawn, C. J. 1971 *J. Fluid Mech.* **48**, 477.

Morrison, G. L., Perry, A. E. & Samuel, A. E. 1972 *J. Fluid Mech.* **52**, 465.

Morrison, W. R. B. & Kronauer, R. E. 1968 *J. Fluid Mech.* **68**, 117.

Perry, A. E. & Morrison, G. L. 1971*a* *J. Fluid Mech.* **47**, 577.

Perry, A. E. & Morrison, G. L. 1971*b* *J. Fluid Mech.* **47**, 765.

Perry, A. E. & Morrison, G. L. 1971*c* *J. Fluid Mech.* **50**, 815.

Squire, H. B. 1948 *Phil. Mag.* **39** (7), 1.

Townes, H. W., Gow, J. L., Powe, R. E. & Weber, N. 1971 *A.S.M.E. Paper*, no. 71-Wa/FE-7.

Townsend, A. A. 1956 *The Structure of Turbulent Shear Flow*. Cambridge University Press.

Wills, J. A. B. 1962 *J. Fluid Mech.* **12**, 388.

Wills, J. A. B. 1964 *J. Fluid Mech.* **20**, 417.

Wyngaard, J. C. 1968 *J. Phys.* E **1**, 1105.